Comparing turbulent flow and bank erosion with controlled experiments in a field-scale meandering channel

Abbreviated Title: Experiments on turbulent flow and bank erosion

J.L Kozarek[1*], A.B. Limaye[2], and E. Arpin[1,3]

[1]St. Anthony Falls Laboratory, University of Minnesota, 2 SE 3rd Ave, Minneapolis, MN 55414, USA

[2]Department of Environmental Sciences, University of Virginia, Clark Hall, 291 McCormick Rd, P.O. Box 400123, Charlottesville, VA 22904, USA

[3]Now at Technische Universität München, Munich, Germany

ORCID ID: JLK, 0000-0001-8913-5646; ABL, 0000-0002-4122-4700

Present addresses: J.L. Kozarek, St. Anthony Falls Laboratory, University of Minnesota, 2 SE 3rd Ave, Minneapolis, MN, 55414, USA

*Corresponding author (e-mail: jkozarek@umn.edu)

Abstract

Bank erosion commonly occurs in alluvial rivers, shaping landscapes and riparian habitats and impacting water quality and infrastructure. Several models have been proposed that link shear stresses to bank erosion. However, data to test these hypotheses for characteristic geometries of meandering channels are sparse and technically challenging to acquire. Here we present results from a controlled experiment in a naturalistic channel to isolate the relationships between turbulent flow and nascent bank erosion. We ran the experiments at the Outdoor StreamLab (St. Anthony Falls Laboratory, University of Minnesota) and gathered high-precision, contemporaneous measurements of the turbulent flow field and topography near a standardized, erodible bank at five locations along a single meander. The measurements show that the rate of bank erosion varied both along the channel and vertically and local bank erosion was not correlated with any single hydrodynamic parameter. Upstream of the meander apex, erosion correlated with the time-averaged streamwise velocity magnitude while downstream of apex, bank erosion correlated more strongly with turbulence parameters and depth. These results support field measurements that suggest that fluid shear contributions to outer bank erosion reflect multiple components of turbulent flow structure in river meanders.

Keywords: geomorphology: fluvial; river channels; erosion; streamflow; turbulence

Introduction

Bank erosion is a common process in alluvial rivers, particularly on the outer banks of meander bends. A common conceptual model for bank erosion involves a multistep process with interacting hydraulic, sediment transport, and geotechnical factors. Flow-driven erosion at the base of the bank can create an undercut that destabilizes the bank, leading to failure (Osman and Thorne 1988; Simon *et al.* 2000; Darby *et al.* 2002; Rousseau *et al.* 2017). Subsequently, an eroded block can temporarily forestall further erosion directly by armoring the bank and indirectly by locally depressing flow velocity and shear stress (Kean and Smith 2006; Eke *et al.* 2014). As bank erosion widens channels, bars also grow outward from the opposite bank. Together, these processes cause the lateral translation of meandering channels while they maintain a relatively constant width – an essential characteristic that remains incompletely understood (Parker *et al.* 2011).

Bank erosion impacts a wide range of Earth-surface phenomena. Erosion enables alluvial channel migration across valley floors over human and geologic timescales (Erkens *et al.* 2009; Blum *et al.* 2013; Constantine *et al.* 2014) and shapes topography (Sun *et al.* 1996). Beyond this geomorphic impact, bank erosion alters riparian habitat (Salo *et al*. 1986), endangers bridges and other infrastructure (Lagasse *et al.* 2004), and degrades water quality by contributing excess sediment and affiliated contaminants to channels (Belmont *et al.* 2011). A major challenge in understanding these processes is relating stress contributions from turbulent flow, which fluctuate over timescales of seconds, to channel evolution over years to decades (Camporeale *et al.* 2005; Keylock 2015; Schwenk et al. 2015). These applications have motivated numerous predictive models that link hydraulics in river meanders and erosion of the outer bank through excess velocity or shear stress (e.g. Ikeda *et al.* 1981; Simon *et al.* 2011; Motta *et al.* 2014). Mechanistic bank retreat models, such as the Bank Stability and Toe Erosion Model (BSTEM) of the USDA-ARS (see Klavon *et al.* 2016) couple geotechnical bank processes with a common approach to predict fluvial erosion rate, ε, the excess shear equation, (Partheniades 1965)

$$\varepsilon = k(\tau_a - \tau_c) \quad (1)$$

where τ_c is the critical shear stress and k is the erodibility coefficient, both properties of the bank material and τ_a is the applied shear stress. In meandering channels, the near-bank shear stress is a function of curvature-induced helical flows that create complex flow and turbulence patterns (Thorne *et al.* 1985).

Field and laboratory studies currently support two opposing mechanisms for the link between turbulent flow and near-bank shear stress (see summary table in Engel and Rhoads 2017). In one case, Blanckaert et al. (2011; 2012) argue that turbulent flow structures reduce turbulent stresses at the outer bank compared to the thalweg. This mechanism, tied to development of a weak counter-rotating cell on the outer bank, is argued to predominate in higher-curvature bends and in some cases reduce channel migration rates. In the second mechanism, turbulent stresses are higher at the outer bank due to topographic steering of the main flow and curvature-induced helical motion (Abad and Garcia 2009a,b; Jamieson *et al.* 2010). Limited field observations of near-bank turbulence are consistent with this second model (Anwar 1986; Engel and Rhoads 2012; Sukhodolov 2012; Engel and Rhoads 2017). These studies highlight the 3-D flow complexity in meander bends, the importance of roughness elements, and the difficulties relating near-bank turbulent flow to bank erosion.

Data to test these models for characteristic geometries of natural channels – with asymmetric, mobile, sediment beds and rough, sloping banks – are sparse. Flow field measurements from laboratory studies often use duct-shaped channels with flat beds, smooth walls, and/or vertical banks (Abad and Garcia 2009b; Jamieson *et al.* 2010; Blanckaert *et al.* 2012). Few studies have tested for specific relationships between near-bank turbulence and outer-bank erosion using measurements in natural meandering channels, wherein bank roughness might disrupt development of coherent flow structures that are typically observed in the laboratory (Engel and Rhoads 2017; Thorne and Furbish 1995). Many studies quantifying flow fields in meandering channels rely on time-averaged measurements; quantifying detailed near-bank 3-D flow and turbulence during erosive flows is challenging due to safety concerns and limitations of instrumentation (Engel and Rhoads 2017). Isolating bank erosion mechanisms is also challenging in the field due to stratification of bank materials (Thorne 1982; Pizzuto 1984; Lauer and Parker 2008) and spatially and temporally variable erodibility (Wynn *et al.* 2008; Constantine *et al.* 2009; Konsoer *et al.* 2016). In addition, bank retreat is often measured at a temporal scale (e.g. via surveying, remote sensing or erosion pins) that incorporates both fluvial erosion and subsequent bank failure creating ambiguity in reconstructing the relative importance of flow-induced erosion. These challenges obscure the relative importance of different mechanisms – including cross-stream and along-stream secondary flow, deflection of the primary flow, turbulent fluctuations, and bank roughness – for explaining near-bank turbulent shear stress and erosion in meandering channels. This uncertainty further limits opportunities to discriminate models for river migration that relate channel planform curvature, flow, and channel migration, over the short (i.e., single event) and long-term (i.e., decadal timescale; Camporeale *et al.* 2007).

Several theoretical models establish links between channel hydro- and morphodynamics and geotechnical properties of the bank (e.g., Simon *et al.* 2000; Eke *et al.* 2014; Lai *et al.* 2015). In this study, we focus on one portion of this multi-step erosion process using an outdoor field-scale experimental stream to elucidate the relationships between turbulent flow and hydraulic bank erosion. We present a set of experiments that leverages the strengths of both controlled experiments (e.g. water and sediment discharge) and of a natural setting with the key characteristics of an alluvial river – most importantly, a meandering channel shape, irregular bed and bank topography, mobile bed sediment, and bank roughness from vegetation. We use this experimental facility to make detailed, contemporaneous measurements of flow and erosion patterns using standardized, homogeneous bank materials. We develop new methods to deploy a weakly cohesive bank material that is susceptible to fluid wear while still sufficiently competent to be installed with a consistent geometry that enables systematic measurements of erosion around a meander bend. We utilize this unique experimental setup to relate various methods of estimating applied bank shear to bank erosion.

Experiment design

Overview: The Outdoor StreamLab

We conducted bank erosion experiments from June to August of 2019 in the Outdoor StreamLab (OSL) adjacent to St. Anthony Falls Laboratory at the University of Minnesota. The OSL consists of a field-scale stream and floodplain built on an abandoned flood bypass channel on the Mississippi River. The OSL has been used to study a variety of ecogeomorphic processes including flow, bed topography, and bedform migration in meandering channels (Kang and Sotiropoulos 2011; Khosronejad *et al.* 2014; Palmsten *et al.* 2015) and feedbacks among these processes in the presence of vegetation (Rominger *et al.* 2010; Kui *et al.* 2014; Lightbody *et al.* 2019).

The OSL includes a 50-meter long, meandering channel with a pool-riffle sequence (approximate width and depth of 2.5 m and 0.3 m, respectively) within a vegetated riparian floodplain (20 m x 40 m; Fig. 1a). The channel planform was constructed in 2008 as a sine-generated curve with moderate sinuosity (1.3) and a wavelength of 25 m, and the banks were initially stabilized with coconut fiber matting overlain with plastic netting. The streambanks were then planted with a mix of native riparian vegetation and the floodplain was seeded with a native prairie seed mix. In 2019, 11 years after channel construction, remnants of the stabilization netting persisted in some areas and in combination with stable vegetative root systems limited overall bank migration. At the time of these experiments, the OSL channel banks were relatively stable with few isolated undercut banks and naturally roughened due to vegetation, while the sediment bed was mobile under bankfull flow. These conditions motivated construction of a standardized erodible bank, as described below.

The OSL streambed consists of a mobile sand ($D_{50} = 0.8 \pm 0.3$ mm) with two constructed riffles (cobbles with diameter 10-15 cm) framing the middle meander. Coarser material ($D \sim 4.7$ mm) is present in the thalweg around the outer portion of this meander bend. Water discharge is controlled by valve from the Mississippi River and monitored continuously by measuring the depth of flow over a weir by a Massa ultrasonic transducer. Sediment ($D_{50} = 0.8 \pm 0.1$ mm) is fed to the upstream end of the channel controlled by a variable-speed auger. Sediment that moves through the channel as bedload is captured in a stilling basin at the downstream end of the channel and is siphoned back to the sediment feeder. With these components, the OSL enables repeatable experiments with controlled water and sediment supply.

The OSL enables several phenomena that mimic flow boundary conditions in natural channels that are not present in most experimental studies. The bankfull flow depth (~0.3 m) is sufficiently deep to transport the fed sediment as migrating dunes (Palmsten *et al.* 2015). The presence of bedforms introduces roughness that impacts the mean flow (Ferguson 2013), but this condition is rarely achieved for laboratory meandering channels (Abad and Garcia 2009a; Termini 2009; Whiting and Dietrich 1993 a,b) In addition to migrating bedforms, the presence of vegetated banks (Rominger *et al.* 2010; Kui *et al.* 2014; Lightbody *et al.* 2019) generates bank roughness conditions typical of small sand-bedded streams.

Topography and flow field measurements

We used a custom instrument carriage to measure channel and bank topography with sub-millimeter ranging accuracy, centimeter-scale spatial resolution, and a field of view of approximately 1.3 m by 1 m in the cross-stream and streamwise directions, respectively (Fig. 1b). The instrumentation carriage is georeferenced within a local OSL coordinate system using Sokkia X30RK total-station surveying and by scanning permanent benchmarks located along the channel. We collected simultaneous elevation measurements of the subaqueous channel bed and the water surface using a downward-looking JSR Ultrasonics sonar and a Massa ultrasonic transducer, respectively. We collected topography for areas above the water surface using a laser range finder (Keyence LK-G series), and measured bank topography at low flow with an adjustable-angle mount for the laser range finder. This mount is adjustable between 0 and 90 degrees to enable measurements approximately normal to the bank face to account for undercutting and near-vertical surfaces (Fig. 1c). Topographic scans from different locations were merged over the entire experiment area in the OSL coordinate system.

As a precursor to the bank erosion experiments, we measured baseline topography and flow patterns under quasi-equilibrium morphodynamic conditions with a constant discharge (300 ± 4 L/s) and sediment feed (6.9 ± 0.5 kg/min.). Sand bedforms developed and migrated under these conditions (Palmsten *et al.* 2015). To account for this variation, we repeated and averaged eight scans to produce time-averaged topography at each carriage location. Velocity and turbulence data were collected at nine cross-sections (XS1 to XS9) using a downward-looking acoustic Doppler velocimeter (ADV; Nortek Vectrino+; Fig. 1a). XS1 and XS9 were located mid-riffle and XS2-XS8 were spaced along the meander. The ADV probe was mounted to a channel-spanning portable traverse with lateral and vertical positioning. At each cross section, the position of this traverse was located within the OSL coordinate system using a total station. At each location, three-dimensional velocity data were collected at 100 Hz for 120 seconds to characterize turbulent flow. Velocity timeseries were evaluated to ensure that mean velocity and turbulence statistics converged over this sampling time. Data were post-processed using a phase-space thresholding method (Parsheh *et al.* 2010).

Erodible bank preparation and deployment

We developed a workflow to create standardized, synthetic banks, overlain on the existing banks in the OSL channel, to systematically control for bank roughness, erodibility, and critical shear stress within the areas of the bank erosion measurements (Fig. 2). We designed these synthetic banks using a cohesive sediment mixture to approximate the materials in a typical alluvial streambank using a well-mixed combination of 90% sand (D_{50} = 0.71 mm) and 10% bentonite clay with 15% moisture content (mixture D_{50} = 0.69 mm). The optimum moisture was determined by a standard proctor compaction test (ASTM D698; Akinola et al. 2019). We formed rectangular sections (0.55 x 0.75 m) of this synthetic bank by pressing the material into a frame (5 cm deep) over a wire-mesh foundation (Fig. 2a). The proportions of sand and bentonite were determined using field tests such that the material was weak enough to perceptibly erode over a typical experimental time window (~ 4 hours), but cohesive enough to prevent complete erosion during this interval and maintain the steep bank geometry (40^{o} – 64^{o}) present in the existing OSL banks.

The bank materials were built up and compacted in four layers to ensure adequate compaction and adhesion to the underlying metal structure (Fig. 2a). The first layer consisted of a very thin layer pressed into the metal frame with a plastic spatula then scored in a cross-hatch pattern to ensure proper joining between layers (Fig. 2b). Three additional layers were added by first compacting using a modified 4.5 kg slide hammer (similar to Hoomehr *et al.* 2018) in a gridded pattern over the surface, then scoring prior to the addition of the next layer (Fig. 2c). After the final compaction (Fig. 2d), the bank was screed flush with the frame (2.5 cm), then carefully removed and trimmed. Because the erodibility of cohesive mixtures has been shown to vary considerably not only with field parameters such as water chemistry and temperature (Akinola *et al.* 2019), but also with sample holding time (Akinola *et al.* 2018), each bank was allowed to equilibrate in an enclosed waterproof bag overnight prior to the experiments with pans of water and saturated sponges to maintain humidity for at least 16 hours. Artificial grass (pile height ~ 2.5 cm) was attached to either side of the synthetic bank to create a gradual roughness transition from vegetation to bare bank and a flexible rubber mat was added along the bottom to form a smooth contact with the streambed (Fig. 3c).

Bank erosion experiments

Five separate experiments were conducted under the same water (300 L/s) and sediment discharge (6.9 ± 0.5 kg/min) conditions in a 10-day window in August 2019. Over this timeframe, water temperature remained relatively constant (24.8 ± 0.6 ºC). For each experiment, we installed one section of the synthetic bank along the outer bank of the middle meander bend of the channel (Fig. 1). We placed the synthetic bank sections at approximately even intervals centered on the apex of the bend to characterize relationships between bank erosion and hydrodynamics that vary systematically with along-stream distance (e.g. Dietrich *et al.* 1983).

To establish the initial position of the synthetic bank section, at low water conditions each bank surface was scanned for topography. Next, we slowly raised the water and sediment discharge over 45 minutes until the target flow was reached (Fig. 3a), avoiding sudden changes in stage height and flow velocity. The target flow was maintained for 3.75 hours. During the experiment, a side-looking ADV (Nortek Vectrino+) was used to collect flow and turbulence near the bank surface and in profiles perpendicular to the bank face (Fig. 3b). Points closest to the bank surface were collected at 100 Hz for 240 seconds while other points were collected at 100 Hz for 120 seconds. ADV data were post-processed identically to the baseline velocity measurements. To conclude each experiment, the flow and sediment feed were turned off, the channel was drained (Fig. 3c), and the synthetic bank was re-scanned for topography. We then removed the synthetic bank in preparation for the next experiment with a new erodible bank (Fig. 3d).

Data analysis

For each experiment, topography scans for the bank before and after flow were gridded to a common coordinate system facing the bank surface with 5 mm grid spacing. The difference between the pre- and post- scans for each bank were calculated by first fitting a plane to the pre-flood bank surface, then detrending by calculating the distance from the plane to each point for the pre- and post-flood surface. Each detrended surface was filtered using an adaptive, low-pass Wiener filter with a 10 x 10 neighborhood. The difference between the two detrended surfaces was then calculated. Over the time frame of the experimental floods (3.75 hours), the bank surface swelled by approximately 2.2-2.5 mm. As all bank erosion measurements were collected perpendicular to the bank face, no correction for swelling was made. Banks D and E shifted slightly during the flood experiments; therefore, the pre-flood surface was adjusted to the post-flood bank surface using an iterative closest point (ICP) method (Bergstrom 2021) before calculating the difference. Because this adjustment may result in underestimating either swelling or erosion compared to banks A-C, banks D and E were analyzed separately.

Instantaneous velocities were decomposed into mean $(\bar{u}, \bar{v}, \bar{w})$ and turbulent fluctuations (u', v', w') in the streamwise, cross-stream, and vertical directions. Shear stress from turbulence kinetic energy was calculated as

$$\tau_{TKE} = \rho C_1 \frac{\left(\overline{u'^2} + \overline{v'^2} + \overline{w'^2}\right)}{2} \quad (2)$$

where ρ is water density and overbar denotes a mean. C_1 is a proportionality constant estimated as 0.19 (Biron et al. 2004; Kim et al. 2000). Shear stresses from Reynolds stresses were calculated with near-bank, fluctuating velocity components

$$\tau_{uv} = -\rho \overline{u'v'} \quad (3a)$$

$$\tau_{uw} = -\rho \overline{u'w'} \quad (3b)$$

$$\tau_{vw} = -\rho\overline{v'w'} \quad (3c)$$

We also calculated shear stress from TKE using a modification of the TKE approach based on the vertical fluctuations to calculate a shear stress

$$\tau_{TKEw} = \rho C\overline{w'w'} \quad (4)$$

where C is an empirical constant often estimated as 0.9 (Biron et al. 2004; Kim et al. 2000). Local differences between pre- and post-flood topography scans were collected in a 4 cm grid around the location of each point measurement of near-bank flow velocity to compare local erosion to turbulent flow parameters.

Results

Baseline topography and flow field

Figure 4 shows the baseline, time-averaged topography and surface velocity vectors at nine cross sections. The bed topography shows a point-bar morphology with a major scour hole entering the bend, just downstream of the constructed riffle area and coincident with XS2. A second scour hole occurs near the outer bank, downstream of the meander apex; its point of deepest scour coincides with XS6, located between banks C and D.

As flow enters the study reach and passes the first major scour hole, along-stream velocity and turbulence statistics are highest mid-channel (XS3 in Fig. 5). This core of high-velocity flow shifts toward the outer bank through XS4, 5, and 6 until XS7. Previous, high resolution computational fluid dynamics (CFD) models of flow in the OSL highlighted the presence of turbulent flow structures (Kang and Sotiropoulos 2011). Though strong secondary currents are visible throughout the meander, the ADV measurements in this study do not resolve a counter-rotating, outer bank cell. Turbulence, described by TKE and Reynolds stresses (-*u*'*w*'), is greatest near the bank toe downstream of the meander apex, consistent with the conceptual model described in Engel and Rhoads (2017).

Near-bank erosion and flow field

Detailed flow patterns were collected in the vicinity of each experimental bank (Fig. 1 and Fig. 6). The streamwise, time-averaged, near-bank velocity increases from bank A to bank C, at the meander apex. Downstream of this point, the high-velocity zone moves away from the bank surface near banks D and E. However, the near-bank turbulence increases at banks D and E, especially near the bank toe.

The bank erosion profiles (Fig. 7) were split into two groups, banks A to C and banks D and E, due to differences in processing described in the data analysis section. Bank A, located upstream of the meander apex, had very little erosion over the synthetic bank. The mean difference between the bank surfaces before and after flow for A was 2.5 mm, indicating slight swelling of the bank material due to submergence in the channel flow. Bank B had an area of minimal erosion near the toe of the bank and an average difference of 0.8 mm. Bank C eroded over much of the bank surface, with mean difference of 0.6 mm. The erosion magnitude of banks D and E cannot be compared directly to banks A-C because the former shifted slightly between the pre-flow and post-flow scans. However, considered by themselves, the patterns of erosion on banks D and E illustrate maximum erosion near the bank toe, coinciding with the areas of high near-bank turbulence (Fig. 6).

Comparison of observations for turbulent flow and bank erosion

A summary of the mean near-bank shear stress estimates from turbulence parameters for each bank are summarized in Table 1. These results show significant variation both for a single estimate (standard deviation) and between estimates of shear stress. Estimates of shear stress varied by an order of magnitude depending on the method used. Estimates of near-bank shear stress were not calculated using the time-averaged velocity and a logarithmic profile because flow fields near the bank did not adequately follow a logarithmic profile near the sloping bank (similar to Hopkinson and Wynn-Thompson 2016)

We compared the near-bank flow and turbulence measurements to the local magnitude of bank erosion in a 4 x 4 cm region. As above, banks A to C were analyzed separately from banks D and E. For banks A to C, as the magnitude of turbulence increased, the erosion increased (Fig. 8); however, these relationships were not significant for any of the turbulence estimates ($\alpha = 0.05$). For A-C, the erosion magnitude was correlated ($\alpha = 0.05$) to the time-averaged streamwise velocity, but not the depth (Fig. 9). Banks A and B were upstream of the meander apex and bank C was located approximately at the meander apex. These results show a pattern of increasing erosion as the high-velocity core of the flow approaches the meander apex.

For banks D and E, located downstream of the meander apex, we calculated the pattern of relative erosion with depth along each banks. There was a significant correlation between depth and erosion magnitude for both banks D and E ($\alpha = 0.05$) and no significant relationships between streamwise or cross-stream velocity and erosion magnitude for either bank (Fig. 10). There was, however, a significant relationship between vertical velocity magnitude and erosion for bank D. In this case, there was more scour for more negative vertical velocity and less for positive vertical velocity. There were no significant relationships between turbulence parameters and erosion magnitude for bank E, but erosion magnitude at bank D was significantly correlated to both Reynolds stress and TKE (Fig. 11). As the magnitude of turbulence increased, the bank erosion increased.

Discussion

For natural channels, comparing turbulent flow parameters to bank erosion over a single flood is complicated by limited access during high flow (Engel and Rhoads 2017), ambiguity in measuring erosion and differentiating its mechanisms, and heterogeneous erodibility of bank materials (Wynn *et al.* 2008; Konsoer *et al.* 2016). Therefore, few studies exist to test the relationship between near-bank shear stress derived from measurable turbulence parameters and fluvial bank erosion as proposed in common theoretical formulations (eqn. 1). Although experiments can potentially address these gaps, replicating natural processes in the laboratory poses different challenges. For example, da Silva and Ebrahimi (2017) present an experiment with velocity and turbulence measurements with a fixed channel bed while allowing the bank material to mobilize. In the field, however, this situation is often reversed with bank material being less erodible than the bed material due to sediment cohesion and vegetation.

The experiments presented in this paper suggest a pathway for addressing these technical limitations for a smallsand-bedded channel. Specifically, we conducted measurements under quasi-equilibrium flow conditions with a mobile bed, used homogenous bank materials that experienced measurable erosion over a single flood, and measured flow and turbulence simultaneously with bank erosion. The application of synthetic, standardized bank materials provides a basis for evaluating erosion patterns for similar experiments on bank erosion, for example, incorporating bank erosion into studies on the feedbacks between channel morphology and vegetation (Lightbody *et al.* 2019).

Flow in the OSL produced curvature-induced secondary circulation and a high-velocity core that migrated toward the outer bank around the meander bend (Fig. 5). These flow patterns in the OSL have been well documented in the development of numerical methods of flow and bed morphodynamics in meandering channels (Kang and Sotiropoulos 2011; Khosronejad *et al.* 2014) and the implications of these complex flows have been studied for a range of ecogeomorphic processes including nutrient dynamics (Guentzel *et al.* 2014), bedform migration (Palmsten *et al.* 2015), emergent vegetation (Lightbody *et al.* 2019), and model turbines (Hill *et al.* 2016). All of these previous studies, however, were conducted under conditions with little to no bank evolution. The influence of not only the large-scale meandering flow patterns, but the near bank flow and turbulence on bank erosion was carefully quantified in these experiments, and the results indicate spatially varying contributions of the mean flow and turbulence to bank erosion depending on the location around the meander bend. Upstream of the meander bend apex, bank erosion was correlated to mean streamwise flow velocity, while downstream of the meander apex, bank erosion was correlated with turbulence parameters, specifically to the cross-stream and vertical contributions to the overall velocity fluctuations (Fig. 8 to 11).

The lack of a consistent relationship between near-bank shear stress estimates from individual turbulent flow statistics and bank erosion patterns around a meander bend has implications for modelling hydraulic bank erosion. The rate of hydraulic erosion is often calculated using the excess shear equation (eqn. 1) relating hydraulic shear stress to the critical shear stress and erodibility of bank materials (see Motta *et al.* 2012b; Klavon *et al.* 2017). The use of this relationship requires appropriate estimates of critical shear stress and soil erodibility for the local bank materials and an appropriate measure of near bank shear stress. The spatial and temporal variability of critical shear stress and erodibility is well documented. These parameters can vary significantly due to heterogeneous bank materials (Motta *et al.* 2012b; Daly *et al.* 2015a; Daly *et al.* 2015b; Lai *et al.* 2015; Konsoer *et al.* 2016; Langendoen *et al.* 2016), subaerial processes (Wynn *et al.* 2008), vegetation (Allen *et al.* 2016) and water and soil chemistry (Hoomehr *et al.* 2018).

Less is known about the impact of the spatial (Engel and Rhoads 2016, 2017) and temporal (Hopkinson and Walburn 2016) distribution of near-bank shear stress on hydraulic bank erosion (Papanicolaou *et al.* 2007) in part due to the challenges in measuring or estimating near-bank shear stress that are highlighted in this study. The selection of an appropriate method of calculating near-bank shear stress can have significant impacts on estimates of bank erosion. Depending on the method used, estimates of near-bank turbulent shear stress in the meandering OSL varied by an order of magnitude (see Table 1); however, even in a straight channel, near-bank shear stress estimates from turbulence parameters can vary greatly based the three-dimensional flow structure created by a sloped bank and the presence of different types of vegetation (Hopkinson and Wynn-Thompson 2016). Within a meandering channel, the curvature-induced secondary flow strongly impacts the distribution of Reynolds stresses near the outer bank (Engel and Rhoads 2017). However, large roughness elements can also interrupt these patterns and can override the reach-scale effects of channel curvature (Engel and Rhoads 2012). This complexity is often not considered or accounted for in models of hydraulic bank erosion (Klavon *et al.* 2017). For example, BSTEM 5.4 (Simon *et al.* 2011) and other bank erosion models use the local depth-slope product to estimate the applied shear stress with a correction factor to account for stream curvature (Crosato 2007) and a correction for effective boundary shear stress due to grain, form, and vegetal components (Temple *et al.* 1987).

To address the spatial distribution of applied shear stress, two-dimensional depth-averaged hydraulic models have been incorporated with the excess shear equation (Lai *et al.* 2015; Motta *et al.* 2012a; Motta *et al.* 2014; Klavon *et al.* 2017). Lai et al. (2015) account for the vertical variation in near-bank shear stress by utilizing the ray-isovel model (Kean and Smith 2006a; Kean and Smith 2006b) to account for form drag due to bank properties such as vegetation. However, these time-and spatially-averaged methods cannot fully account for the three-dimensional flow structure and turbulence fluctuations that drive sediment motion (Yager *et al.* 2018) and thus are limited in accurately predicting the spatial variation of bank erosion due to fluid forces. The results of this study indicate that the flow patterns responsible for bank erosion vary around a single meander bend. Upstream of the meander apex to the meander apex, bank erosion was most closely related to mean streamwise velocity while downstream of the apex, turbulence near the bank toe was correlated to zones of higher bank erosion. Further experiments across a range of meander planform geometries could establish whether these observations can be generalized for use in bank erosion modelling.

Conclusions

We used controlled experiments in a meandering channel to isolate the relationships between turbulent flow and fluvial bank erosion. Contemporaneous measurements of the turbulent flow field and erosion of a standardized, erodible bank allow us to directly evaluate the effect of fluid forces on bank erosion while controlling for the complexity of bank erodibility and critical shear stress due to heterogeneous bank materials. The results of this study highlight the complexity and challenges of measuring and modeling the near bank fluid forces that lead to bank erosion in natural meandering channels with mobile bedload, vegetation, and complex channel morphology and indicate that the key fluid forces (mean or turbulent flow) responsible for erosion may vary along the meander bend. We did not observe an estimate of near-bank shear stress that consistently correlated with measured bank erosion at all locations along the channel adding to the uncertainty in bank erosion predictions. Instead, bank erosion correlated with mean streamwise flow velocity upstream of the meander bend apex, then correlated with turbulence parameters downstream of the meander apex. These results highlight the need for careful consideration of appropriate near bank shear stress estimates when calculating bank erosion. This study represents a single channel geometry in a controlled but naturalistic setting. The results suggest that further experiments that relate controlled measurements of turbulent flow and bank erosion across a range of materials, and bank and channel geometries can establish improved measures of near-bank shear stress to predict to nascent bank erosion.

Acknowledgments

We thank Blaise Villaume, Nikhil Khurana, Noah Slade, and Nick Bentelspacher for assisting with the experiments and data analysis. SAFL technical staff including Dick Christopher, Ben Erickson, and Erick Steen provided invaluable technical assistance. We would also like to thank Kory Konsoer and an anonymous reviewer for their feedback that greatly improved the manuscript.

Author contributions

J.L. Kozarek: Conceptualization (equal), Investigation (lead), Formal Analysis (lead), Methodology, Supervision, Visualization, Writing- original draft, Data Curation. **A.B. Limaye:** Conceptualization (equal), Writing – original draft, Writing – review & editing. **E. Arpin:** Methodology, Investigation, Formal Analysis (supporting), Writing – review & editing (supporting).

Funding information

The National Science Foundation (grant EAR-1823530) supported this work.

Data availability

The datasets generated during and/or analyzed during the current study are available in the Data Repository for University of Minnesota repository, https://conservancy.umn.edu/handle/11299/166578.

References

Abad, J.D. and Garcia, M.H. 2009a. Experiments in a high-amplitude Kinoshita meandering channel: 2. Implications of bend orientation on bed morphodynamics. *Water Resources Research*, **45**, https://doi.org/10.1029/2008wr007017.

Abad, J.D. and Garcia, M.H. 2009b. Experiments in a high-amplitude Kinoshita meandering channel: 1. Implications of bend orientation on mean and turbulent flow structure. *Water Resources Research*, **45**, 19, https://doi.org/W02401/10.1029/2008wr007016.

Akinola, A.I., Thompson, T.W., Olgun, C.G., Mostaghimi, S. and Eick, M.J. 2019. Fluvial Erosion Rate of Cohesive Streambanks Is Directly Related to the Difference in Soil and Water Temperatures. *Journal of Environmental Quality*, **48**, 1741-1748, https://doi.org/10.2134/jeq2018.10.0385.

Akinola, A.I., Wynn-Thompson, T., Olgun, C.G., Cuceoglu, F. and Mostaghimi, S. 2018. Influence of Sample Holding Time on the Fluvial Erosion of Remolded Cohesive Soils. *Journal of Hydraulic Engineering*, **144**, https://doi.org/10.1061/(asce)hy.1943-7900.0001504.

Allen, D.C., Cardinale, B.J. and Wynn-Thompson, T. 2016. Plant biodiversity effects in reducing fluvial erosion are limited to low species richness. *Ecology*, **97**, 17-24, https://doi.org/10.1890/15-0800.1.

Anwar, H.O. 1986. Turbulent Structure in a River Bend. *Journal of Hydraulic Engineering,* **112,** 657-669.

Belmont, P., Gran, K.B. *et al.* 2011. Large Shift in Source of Fine Sediment in the Upper Mississippi River. *Environmental Science & Technology*, **45**, 8804-8810, https://doi.org/10.1021/es2019109.

Bergström, P. 2021. Iterative Closest Point Method (https://www.mathworks.com/matlabcentral/fileexchange/12627-iterative-closest-point-method), MATLAB Central File Exchange. Retrieved November 10, 2021.

Blanckaert, K. 2011. Hydrodynamic processes in sharp meander bends and their morphological implications. *Journal of Geophysical Research-Earth Surface*, **116**, https://doi.org/10.1029/2010jf001806.

Blanckaert, K., Duarte, A., Chen, Q. and Schleiss, A.J. 2012. Flow processes near smooth and rough (concave) outer banks in curved open channels. *Journal of Geophysical Research-Earth Surface*, **117**, https://doi.org/10.1029/2012jf002414.

Blum, M., Martin, J., Milliken, K. and Garvin, M. 2013. Paleovalley systems: Insights from Quaternary analogs and experiments. *Earth-Science Reviews*, **116**, 128-169, https://doi.org/10.1016/j.earscirev.2012.09.003.

Camporeale, C., Perona, P., Porporato, A. and Ridolfi, L. 2005. On the long-term behavior of meandering rivers. *Water Resources Research*, **41**, https://doi.org/10.1029/2005wr004109.

Camporeale, C., Perona, P., Porporato, A. and Ridolfi, L. 2007. Hierarchy of models for meandering rivers and related morphodynamic processes. *Reviews of Geophysics*, **45**, https://doi.org/10.1029/2005rg000185.

Constantine, C.R., Dunne, T. and Hanson, G.J. 2009. Examining the physical meaning of the bank erosion coefficient used in meander migration modeling. *Geomorphology*, **106**, 242-252, https://doi.org/10.1016/j.geomorph.2008.11.002.

Constantine, J.A., Dunne, T., Ahmed, J., Legleiter, C. and Lazarus, E.D. 2014. Sediment supply as a driver of river meandering and floodplain evolution in the Amazon Basin. *Nature Geoscience*, **7**, 899-903, https://doi.org/10.1038/ngeo2282.

Crosato, A. 2007. Effects of smoothing and regridding in numerical meander migration models. *Water Resources Research*, **43**, https://doi.org/10.1029/2006wr005087.

da Silva, A.M.F. and Ebrahimi, M. 2017. Meandering Morphodynamics: Insights from Laboratory and Numerical Experiments and Beyond. *Journal of Hydraulic Engineering*, **143**, https://doi.org/10.1061/(asce)hy.1943-7900.0001324.

Daly, E.R., Fox, G.A., Al-Madhhachi, A.S.T. and Storm, D.E. 2015a. Variability of fluvial erodibility parameters for streambanks on a watershed scale. *Geomorphology*, **231**, 281-291, https://doi.org/10.1016/j.geomorph.2014.12.016.

Daly, E.R., Fox, G.A., Enlow, H.K., Storm, D.E. and Hunt, S.L. 2015b. Site-scale variability of streambank fluvial erodibility parameters as measured with a jet erosion test. *Hydrological Processes*, **29**, 5451-5464, https://doi.org/10.1002/hyp.10547.

Darby, S.E., Alabyan, A.M. and Van de Wiel, M.J. 2002. Numerical simulation of bank erosion and channel migration in meandering rivers. *Water Resources Research*, **38**, https://doi.org/10.1029/2001wr000602.

Eke, E., Parker, G. and Shimizu, Y. 2014. Numerical modeling of erosional and depositional bank processes in migrating river bends with self-formed width: Morphodynamics of bar push and bank pull. *Journal of Geophysical Research-Earth Surface*, **119**, 1455-1483, https://doi.org/10.1002/2013jf003020.

Engel, F.L. and Rhoads, B.L. 2012. Interaction among mean flow, turbulence, bed morphology, bank failures and channel planform in an evolving compound meander loop. *Geomorphology*, **163**, 70-83, https://doi.org/10.1016/j.geomorph.2011.05.026.

Engel, F.L. and Rhoads, B.L. 2016. Three-dimensional flow structure and patterns of bed shear stress in an evolving compound meander bend. *Earth Surface Processes and Landforms*, **41**, 1211-1226, https://doi.org/10.1002/esp.3895.

Engel, F.L. and Rhoads, B.L. 2017. Velocity profiles and the structure of turbulence at the outer bank of a compound meander bend. *Geomorphology*, **295**, 191-201, https://doi.org/10.1016/j.geomorph.2017.06.018.

Erkens, G., Dambeck, R. *et al.* 2009. Fluvial terrace formation in the northern Upper Rhine Graben during the last 20 000 years as a result of allogenic controls and autogenic evolution. *Geomorphology*, **103**, 476-495, https://doi.org/10.1016/j.geomorph.2008.07.021.

Ferguson, R. 2013. Reach-scale flow resistance*, In Treatise on Geomorphology, Fluvial Geomorphol.*, **9**, Schroder, J. and Wohl, E., pp. 50–68, Elsevier, San Diego.

Guentzel, K.S., Hondzo, M., Badgley, B.D., Finlay, J.C., Sadowsky, M.J. and Kozarek, J.L. 2014. Measurement and Modeling of Denitrification in Sand-Bed Streams under Various Land Uses. *Journal of Environmental Quality*, **43**, 1013-1023, https://doi.org/10.2134/jeq2013.06.0249.

Hill, C., Kozarek, J., Sotiropoulos, F. and Guala, M. 2016. Hydrodynamics and sediment transport in a meandering channel with a model axial-flow hydrokinetic turbine. *Water Resources Research*, **52**, 860-879, https://doi.org/10.1002/2015wr017949.

Hoomehr, S., Akinola, A.I., Wynn-Thompson, T., Garnand, W. and Eick, M.J. 2018. Water Temperature, pH, and Road Salt Impacts on the Fluvial Erosion of Cohesive Streambanks. *Water*, **10**, https://doi.org/10.3390/w10030302.

Hopkinson, L.C. and Walburn, C.Z. 2016. Near-boundary velocity and turbulence in depth-varying stream flows. *Environmental Fluid Mechanics*, **16**, 559-574, https://doi.org/10.1007/s10652-015-9440-1.

Hopkinson, L.C. and Wynn-Thompson, T.M. 2016. Comparison of Direct and Indirect Boundary Shear Stress Measurements along Vegetated Streambanks. *River Research and Applications*, **32**, 1755-1764, https://doi.org/10.1002/rra.3010.

Ikeda, S., Parker, G. and Sawai, K. 1981. Bend theory of river meanders. Part 1. Linear development, J. Fluid Mech., 112, 363–377.

Jamieson, E.C., Post, G. and Rennie, C.D. 2010. Spatial variability of three-dimensional Reynolds stresses in a developing channel bend. *Earth Surface Processes and Landforms*, **35**, 1029-1043, https://doi.org/10.1002/esp.1930.

Kang, S. and Sotiropoulos, F. 2011. Flow phenomena and mechanisms in a field-scale experimental meandering channel with a pool-riffle sequence: Insights gained via numerical simulation. *Journal of Geophysical Research-Earth Surface*, **116**, https://doi.org/10.1029/2010jf001814.

Kean, J.W. and Smith, J.D. 2006. Form drag in rivers due to small-scale natural topographic features: 1. Regular sequences. *Journal of Geophysical Research-Earth Surface*, **111**, https://doi.org/10.1029/2006jf000467.

Kean, J.W. and Smith, J.D. 2006a. Form drag in rivers due to small-scale natural topographic features: 1. Regular sequences. *J. Geophys. Res.*, 111, F04009, doi:10.1029/2006JF000467

Kean, J.W. and Smith, J.D. 2006b. Form drag in rivers due to small-scale natural topographic features: 2. Irregular sequences. *J. Geophys. Res*., 111, F04010, doi:10.1029/2006JF000490

Keylock, C.J. 2015. Flow resistance in natural, turbulent channel flows: The need for a fluvial fluid mechanics. *Water Resources Research*, **51**, 4374-4390, https://doi.org/10.1002/2015wr016989.

Khosronejad, A., Kozarek, J.L. and Sotiropoulos, F. 2014. Simulation-Based Approach for Stream Restoration Structure Design: Model Development and Validation. *Journal of Hydraulic Engineering*, **140**, https://doi.org/10.1061/(asce)hy.1943-7900.0000904.

Klavon, K., Fox, G., Guertault, L., Langendoen, E., Enlow, H., Miller, R. and Khanal, A. 2017. Evaluating a process-based model for use in streambank stabilization: insights on the Bank Stability and Toe Erosion Model (BSTEM). *Earth Surface Processes and Landforms*, **42**, 191-213, https://doi.org/10.1002/esp.4073.

Konsoer, K.M., Rhoads, B.L., Langendoen, E.J., Best, J.L., Ursic, M.E., Abad, J.D. and Garcia, M.H. 2016. Spatial variability in bank resistance to erosion on a large meandering, mixed bedrock-alluvial river. *Geomorphology*, **252**, 80-97, https://doi.org/10.1016/j.geomorph.2015.08.002.

Konsuer, K.M., Rhoads, B.L., Langendoen, E.J., Best, J.L., Ursic, M.E., Abad, J.D. and Garcia, M.H. 2016. Spatial variability in bank resistance to erosion on a large meandering, mixed bedrock-alluvial river. *Geomorphology*, **252**, 80-97, https://doi.org/10.1016/j.geomorph.2015.08.002.

Kui, L., Stella, J.C., Lightbody, A. and Wilcox, A.C. 2014. Ecogeomorphic feedbacks and flood loss of riparian tree seedlings in meandering channel experiments. *Water Resources Research*, **50**, 9366-9384, https://doi.org/10.1002/2014wr015719.

Lagasse, P.F., Zevenbergen, L.W., Spitz, W.J., and Thorne, C.R. 2004. *Methodology for predicting channel migration*, Transportation Research Board of the National Academies, doi:10.17226/23352.

Lai, Y.G., Thomas, R.E., Ozeren, Y., Simon, A., Greimann, B.P. and Wu, K.W. 2015. Modeling of multilayer cohesive bank erosion with a coupled bank stability and mobile-bed model. *Geomorphology*, **243**, 116-129, https://doi.org/10.1016/j.geomorph.2014.07.017.

Langendoen, E.J., Mendoza, A. *et al.* 2016. Improved numerical modeling of morphodynamics of rivers with steep banks. *Advances in Water Resources*, **93**, 4-14, https://doi.org/10.1016/j.advwatres.2015.04.002.

Lauer, J.W. and Parker, G. 2008. Net local removal of floodplain sediment by river meander migration. *Geomorphology*, **96**, 123-149, https://doi.org/10.1016/j.geomorph.2007.08.003.

Lightbody, A.F., Kui, L., Stella, J.C., Skorko, K.W., Bywater-Reyes, S. and Wilcox, A.C. 2019. Riparian Vegetation and Sediment Supply Regulate the Morphodynamic Response of an Experimental Stream to Floods. *Frontiers in Environmental Science*, **7**, 14, https://doi.org/10.3389/fenvs.2019.00040.

Motta, D., Abad, J.D., Langendoen, E.J. and Garcia, M.H. 2012a. A simplified 2D model for meander migration with physically-based bank evolution. *Geomorphology*, **163**, 10-25, https://doi.org/10.1016/j.geomorph.2011.06.036.

Motta, D., Abad, J.D., Langendoen, E.J. and Garcia, M.H. 2012b. The effects of floodplain soil heterogeneity on meander planform shape. *Water Resources Research*, **48**, https://doi.org/10.1029/2011wr011601.

Motta, D., Langendoen, E.J., Abad, J.D. and Garcia, M.H. 2014. Modification of meander migration by bank failures. *Journal of Geophysical Research-Earth Surface*, **119**, 1026-1042, https://doi.org/10.1002/2013jf002952.

Osman, A.M. and Thorne, C.R. 1988. RIVERBANK STABILITY ANALYSIS .1. THEORY. *Journal of Hydraulic Engineering-Asce*, **114**, 134-150, https://doi.org/10.1061/(asce)0733-9429(1988)114:2(134).

Palmsten, M.L., Kozarek, J.L. and Calantoni, J. 2015. Video observations of bed form morphodynamics in a meander bend. *Water Resources Research*, **51**, 7238-7257, https://doi.org/10.1002/2014wr016321.

Papanicolaou, A.N., Elhakeem, M. and Hilldale, R. 2007. Secondary current effects on cohesive river bank erosion. *Water Resources Research*, **43**, https://doi.org/10.1029/2006wr005763.

Parker, G., Shimizu, Y. *et al.* 2011. A new framework for modeling the migration of meandering rivers. *Earth Surface Processes and Landforms*, **36**, 70-86, https://doi.org/10.1002/esp.2113.

Parsheh, M., Sotiropoulos, F. and Porte-Agel, F. 2010. Estimation of Power Spectra of Acoustic-Doppler Velocimetry Data Contaminated with Intermittent Spikes. *Journal of Hydraulic Engineering*, **136**, 368-378, https://doi.org/10.1061/(asce)hy.1943-7900.0000202.

Pizzuto, J. E. 1984. Equilibrium bank geometry and the width of shallow sandbed streams. *Earth Surface Processes and Landforms,* **9**, 199-207.

Rominger, J.T., Lightbody, A.F. and Nepf, H.M. 2010. Effects of Added Vegetation on Sand Bar Stability and Stream Hydrodynamics. *Journal of Hydraulic Engineering-Asce*, **136**, 994-1002, https://doi.org/10.1061/(asce)hy.1943-7900.0000215.

Rousseau, Y.Y., Van de Wiel, M.J. and Biron, P.M. 2017. Simulating bank erosion over an extended natural sinuous river reach using a universal slope stability algorithm coupled with a morphodynamic model. *Geomorphology*, **295**, 690-704, https://doi.org/10.1016/j.geomorph.2017.08.008.

Salo, J., Kalliola, R., Häkkinen, I., Mäkinen, Y., Niemelä, P., Puhakka, M., and Coley, P.D. 1986. River dynamics and the diversity of Amazon lowland forest. *Nature*, **322**, 254–258, doi:10.1038/322254a0.

Schwenk, J., Lanzoni, S., and Foufoula-Georgiou, E. 2015. The life of a meander bend: Connecting shape and dynamics via analysis of a numerical model. J*. Geophys. Res. Earth Surf.,* 120, 690– 710, doi: 10.1002/2014JF003252.

Simon, A., Curini, A., Darby, S.E. and Langendoen, E.J. 2000. Bank and near-bank processes in an incised channel. *Geomorphology*, **35**, 193-217, https://doi.org/10.1016/s0169-555x(00)00036-2.

Simon, A., Pollen-Bankhead, N. and Thomas, R.E. 2011. Development and Application of a Deterministic Bank Stability and Toe Erosion Model for Stream Restoration. *Stream Restoration in Dynamic Fluvial Systems: Scientific Approaches, Analyses, and Tools*, **194**, 453-474, https://doi.org/10.1029/2010gm001006.

Sukhodolov, A.N. 2012. Structure of turbulent flow in a meander bend of a lowland river. *Water Resources Research*, **48**, https://doi.org/10.1029/2011wr010765.

Sun, T., Meakin, P., Jossang, T. and Schwarz, K. 1996. A simulation model for meandering rivers. *Water Resources Research*, **32**, 2937-2954, https://doi.org/10.1029/96wr00998.

Temple, D.M., Robinson, K.M., Ahring, R.M., and Davis, A.G. 1987. *Stability design of grass-lined open channels*. Agriculture handbook 667, U.S. Department of Agriculture, Stillwater, Oklahoma.

Termini, D. 2009. Experimental observations of flow and bed processes in large-amplitude meandering flume*. Journal of Hydraulic Engineering*, 135(7), 575-587.

Thorne C. R.1982. Processes and mechanisms of river bank erosion, *In Gravel-bed Rivers*, Hey RD, Bathurst JC, Thorne CR (eds.), John Wiley and Sons, Chichester, 227–271.

Thorne C.R, 1982. Processes and mechanisms of river bank erosion, *in Gravel-bed Rivers*, Hey, R.D., Bathurst, J.C., Thorne, C.R. (eds.), John Wiley and Sons, Chichester, 227–271.

Thorne, C., Zevenbergen, L., Pitlick, J. et al. 1985. Direct measurements of secondary currents in a meandering sand-bed river. *Nature*, 315, 746–747, doi:10.1038/315746a0

Thorne, S.D., and Furbish, D.J. 1995. Influences of coarse bank roughness on flow within a sharply curved river bend. *Geomorphology*, 12(3), 241-257.

Whiting, P.J., and Dietrich, W.E. 1993a. Experimental studies of bed topography and flow patterns in large-amplitude meanders: 1. Observations, *Water Resour. Res*., 29(11), 3605– 3614, doi:10.1029/93WR01755.

Whiting, P.J., and Dietrich, W.E. 1993b. Experimental Studies of bed topography and flow patterns in large-amplitude meanders: 2. Mechanisms, *Water Resour. Res.*, 29(11), 3615– 3622, doi:10.1029/93WR01756.

Wynn, T.M., Henderson, M.B. and Vaughan, D.H. 2008. Changes in streambank erodibility and critical shear stress due to subaerial processes along a headwater stream, southwestern Virginia, USA. *Geomorphology*, **97**, 260-273, https://doi.org/10.1016/j.geomorph.2007.08.010.

Yager, E.M., Venditti, J.G., Smith, H.J. and Schmeeckle, M.W. 2018. The trouble with shear stress. *Geomorphology*, **323**, 41-50, https://doi.org/10.1016/j.geomorph.2018.09.008.

Figures

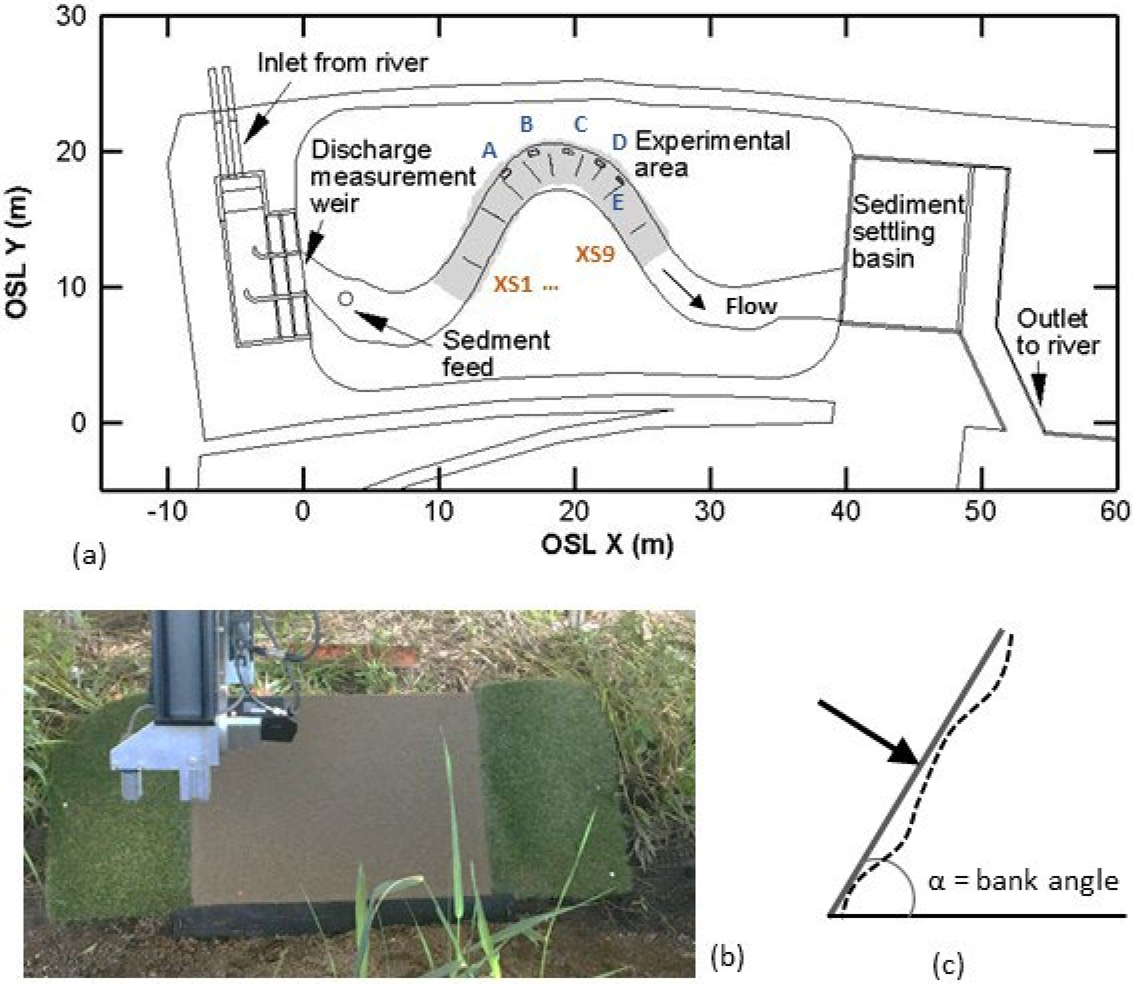

Figure 1. Experimental setup at the Outdoor StreamLab (OSL), St. Anthony Falls Laboratory, University of Minnesota. (a) Plan view of the OSL. Annotations within the channel indicate the area scanned for baseline topography (gray; Fig. 4), the locations of synthetic banks (rectangles and blue letters) and flow velocity cross sections (lines numbered from XS1 in upstream riffle to XS9 in downstream riffle). (b) View of the topography scanner targeting a section of synthetic streambank. (c) Schematic of bank position change measurements using the topography scanner perpendicular to bank face.

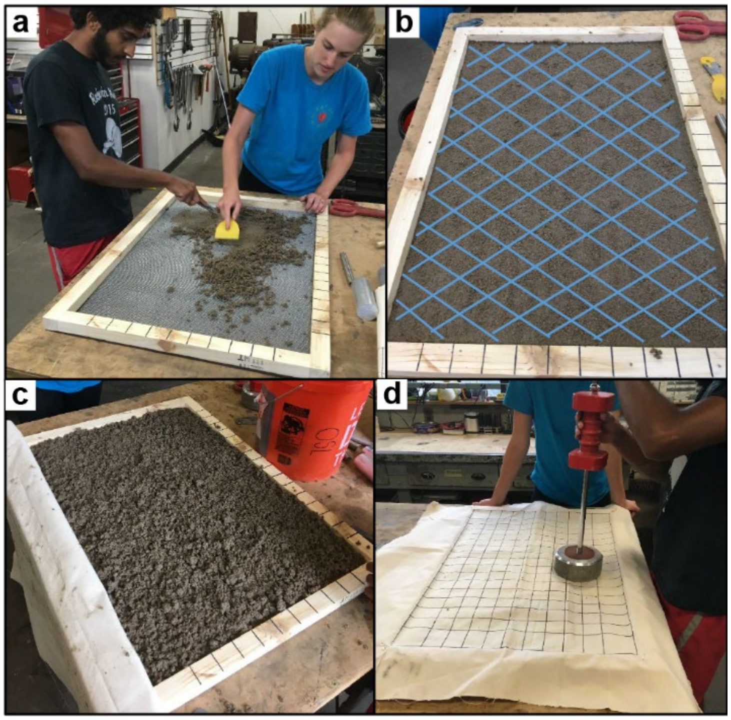

Figure 2. The synthetic bank construction process. (a) A fine layer of the bank mixture is pressed into a metal mesh. (b) The surface is scored in a cross-hatch pattern. (c) One third of the remaining mix is added. (d) The bank mix is uniformly compacted with modified 4.5 kg slide hammer. Steps b-d are repeated twice more.

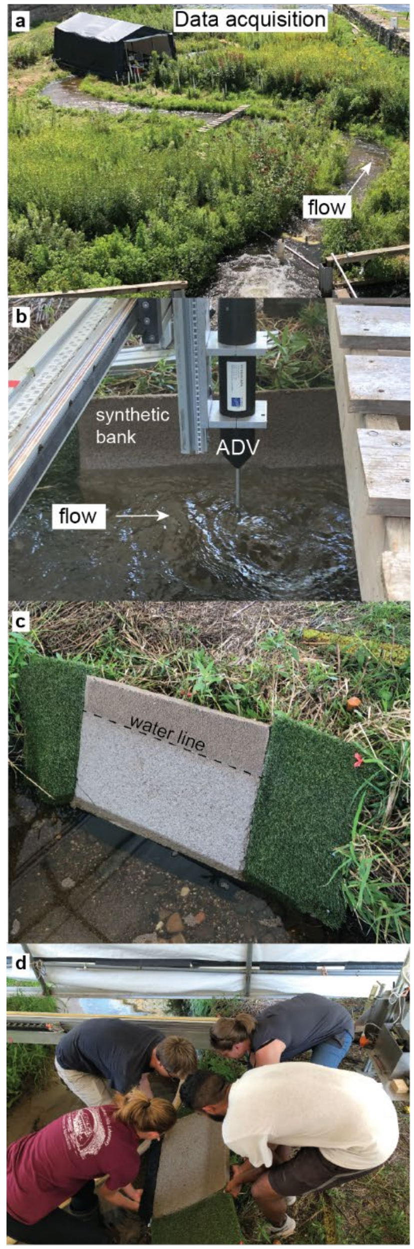

Figure 3. Summary of the experiment workflow. (a) Context image for bank erosion experiments. View is oriented downstream from the inlet, and shows the data acquisition tent located over the channel. (b) The synthetic river bank installed on the edge of the channel. An acoustic Doppler velocimeter (ADV) is immersed in the flow near the bank. (c) After the observation period, the drained channel reveals erosion in the synthetic bank material below the water line. (d) The

synthetic bank is removed from the channel in preparation for the next set of measurements at a different location along the meander bend.

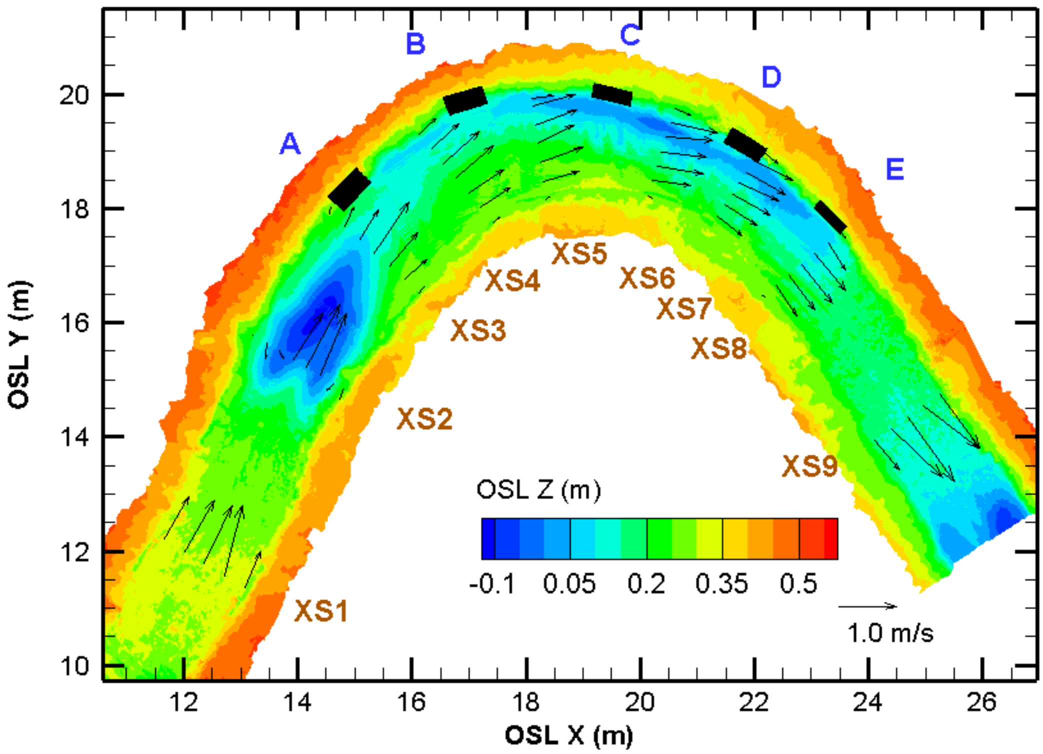

Figure 4. Channel bed and bank topography (colors) with time-averaged surface velocity vectors at each ADV cross-section, labeled XS1 to XS9. XS1 and XS9 are in the constructed riffles framing the bend.

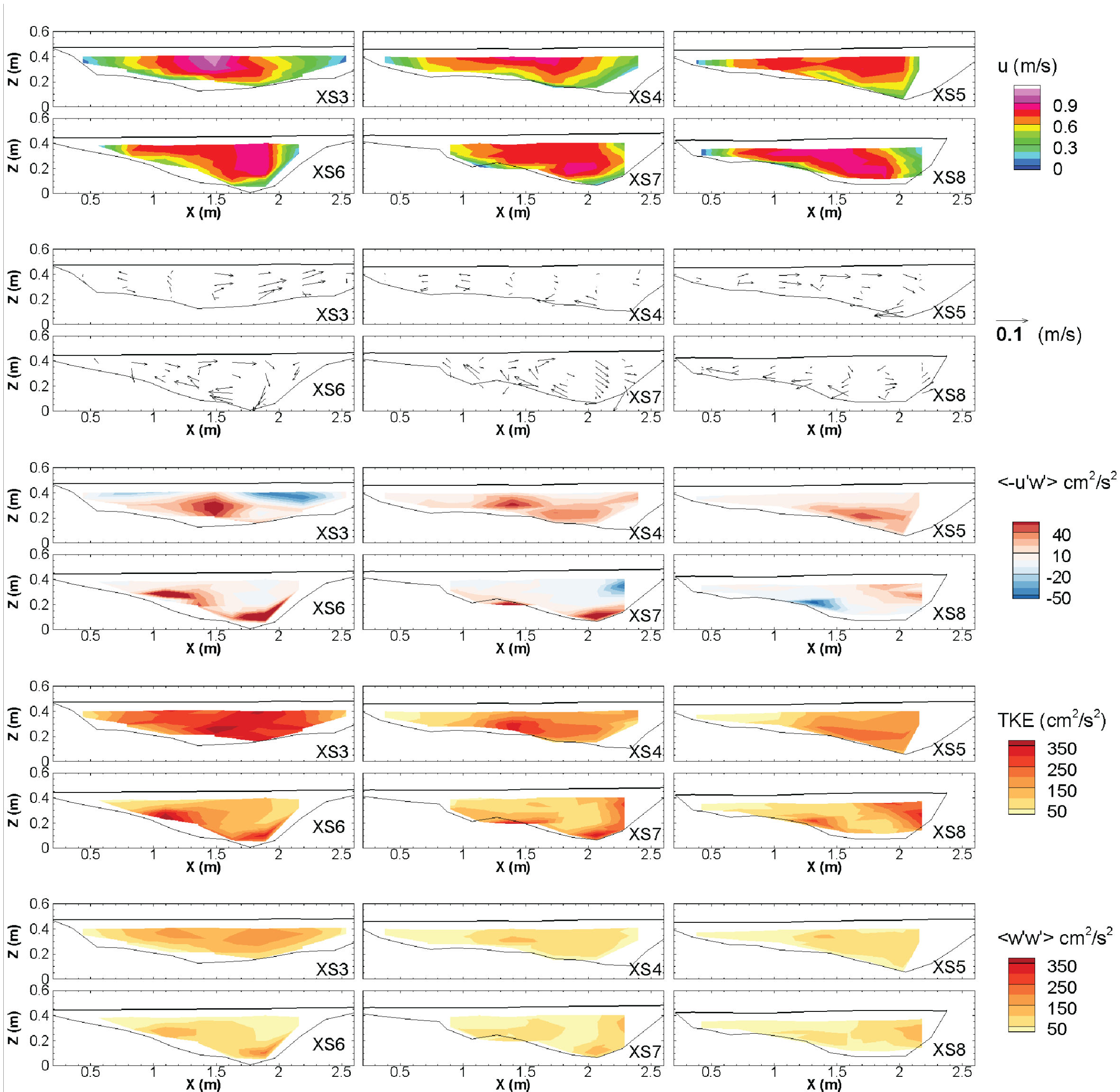

Figure 5. Mean streamwise velocity (*u*), magnitude and direction of cross-stream and vertical velocity, Reynolds stress (-*u*'*w*'), turbulence kinetic energy (TKE) and TKE_w (*w*'*w*') from vertical velocity fluctuations for baseline cross-sections (see Fig.4).

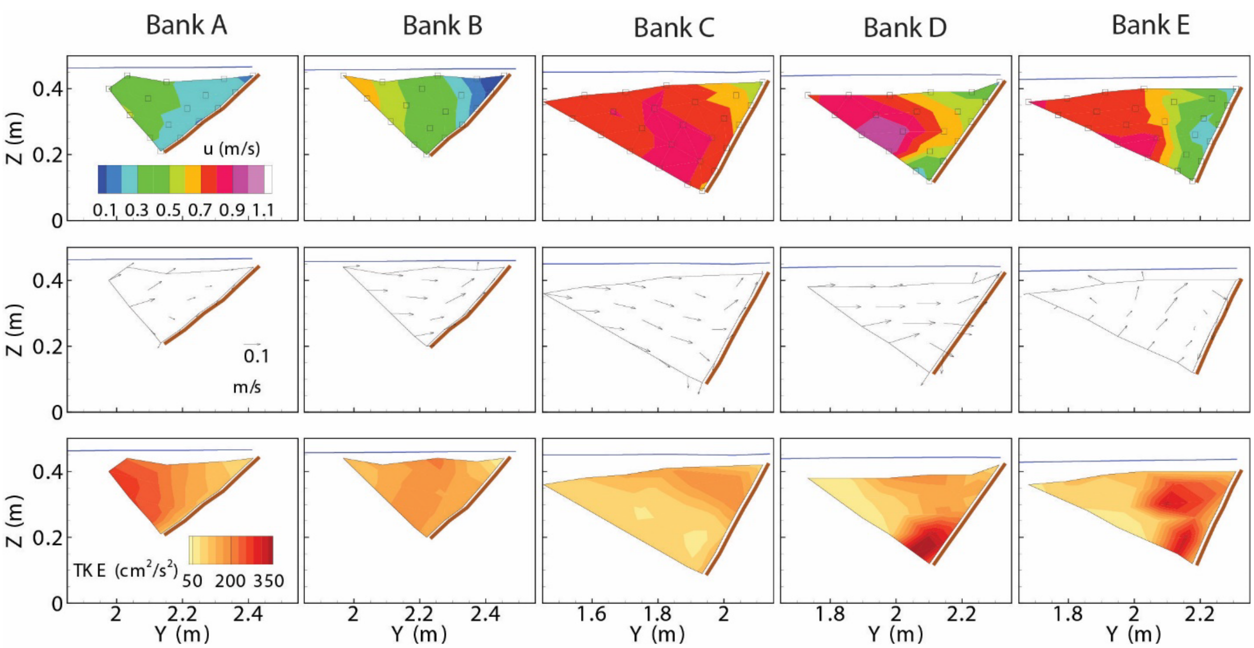

Figure 6. Velocity flow patterns in the vicinity of experimental banks (bank A to bank E). Mean streamwise velocity (*u*, first row), magnitude and direction of cross-stream and vertical velocity (middle row) and turbulence kinetic energy (TKE, bottom row).

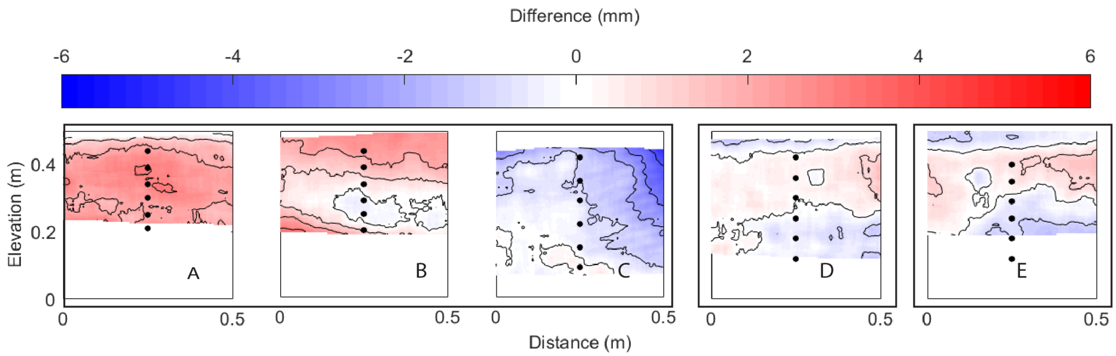

Figure 7. Difference between pre- and post- detrended banks. Dots show locations of ADV measurements. Note that banks D and E shifted slightly during the experiment and cannot be directly compared to banks A-C.

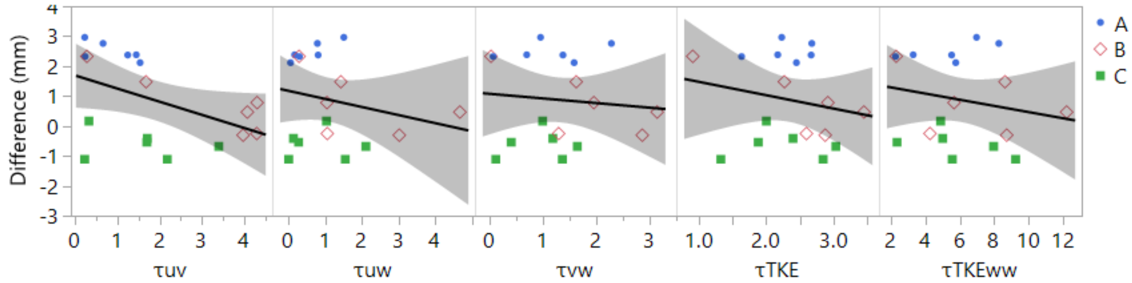

Figure 8. Overall relationships between erosion magnitude and shear stress magnitude (Pa) from turbulence for banks A-C. Shaded area indicates 95% confidence interval for the linear regression fit. No relationships were significant ($\alpha = 0.05$).

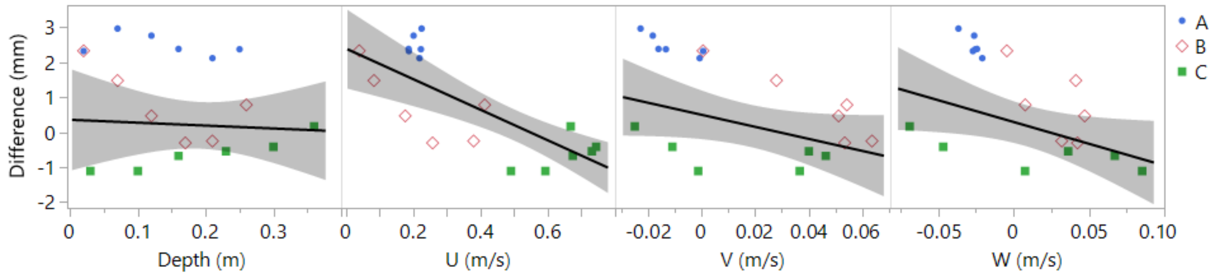

Figure 9. Overall relationships between erosion magnitude (difference between pre- and post-surfaces) and depth, and time-averaged streamwise, cross-stream, and vertical velocity (*U*, *V*, and *W*, respectively) for banks A-C. Shaded area indicates 95% confidence interval for the linear regression fit (significant relationships for *U* and *W*; *p*-value = 0.0004, 0.045, respectively).

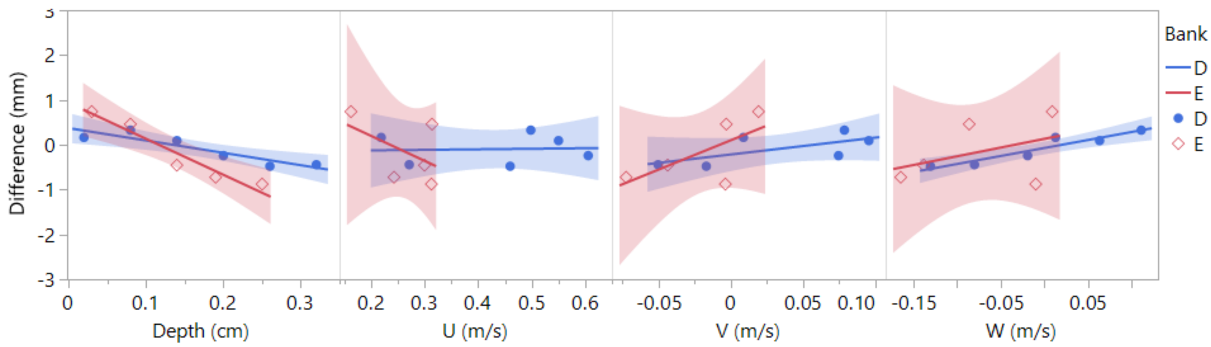

Figure 10. Overall relationships between erosion magnitude and depth, and time-averaged streamwise, cross-stream, and vertical velocity (*U*, *V*, and *W*, respectively) for banks D-E. Shaded area indicates 95% confidence interval for the linear regression fit. The linear regression for depth was significant for both banks D and E (*p*-value = 0.01 and 0.009, respectively) and the regression for W was significant for bank D only (*p*-value = 0.005).

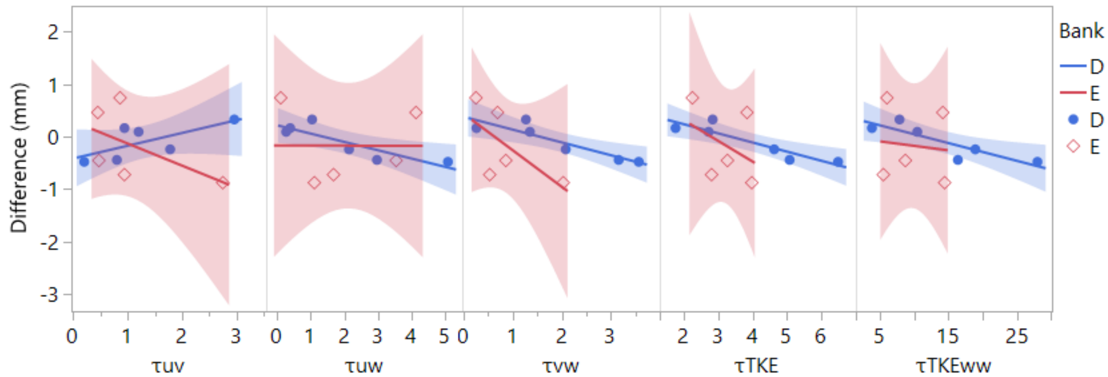

Figure 11. Overall relationships between erosion magnitude and shear stress magnitude (Pa) from turbulence for banks D-E. Shaded area indicates 95% confidence interval for the linear regression fit. The regression for shear stress was significant for bank D for τ_{uw}, τ_{vw}, τ_{TKE}, and τ_{TKEww} (*p*-value = 0.03, 0.01, 0.01, and 0.02, respectively). No regressions were significant for bank E.

Tables

Table 1. Summary of bank experiment results for each bank location. Difference between pre- and post- bank position was calculated from a 4 cm x 4 cm grid surrounding each near-bank flow velocity measurement. Angle is the bank angle relative to horizontal (Fig. 1). Values of difference, velocity, and stress are means (standard deviation in parentheses)

	Bank A	Bank B	Bank C	Bank D	Bank E
Angle (°)	40	47	59	55	64
Difference (mm)	2.5 (0.3)	0.8 (1.0)	-0.6 (0.5)	-0.1 (0.3)*	-0.2 (0.7)*
u (m/s)	0.21 (0.02)	0.22 (0.15)	0.65 (0.09)	0.43 (0.16)	0.27 (0.06)
v (m/s)	-0.01 (0.01)	0.04 (0.02)	0.01 (0.03)	0.03 (0.06)	-0.01 (0.04)
w (m/s)	-0.03 (0.01)	0.03 (0.02)	0.01 (0.06)	-0.01 (0.09)	-0.06 (0.08)
τ_{UW} (Pa)	0.5 (0.6)	-1.8 (1.8)	-0.5 (1.2)	1.6 (2.2)	1.8 (1.7)
τ_{UV} (Pa)	-0.9 (0.6)	-3.1 (1.7)	-1.6 (1.2)	-1.2 (1.1)	-1.0 (1.7)
τ_{VW} (Pa)	1.2 (0.8)	1.8 (1.1)	0.9 (0.6)	1.9 (1.2)	1.0 (0.9)
τ_{TKE} (Pa)	2.3 (0.4)	2.5 (0.9)	2.2 (0.6)	3.9 (1.8)	3.2 (0.6)
τ_{TKEw} (Pa)	5.3 (2.2)	7.0 (3.6)	5.8 (2.5)	14.2 (8.7)	9.8 (3.9)

*The difference between pre- and post- bank position for banks D and E cannot be directly compared to banks A-C due to differences in data processing.